1	HIWIND Balloon and Antarctica Jang Bogo FPI High Latitude Conjugate Thermospheric Wind
2	Observations and Simulations
3	Qian Wu, Dong Lin, Wenbing Wang, Liying Qian
4	HAO/NCAR
5	3090 Center Green Dr.
6	Boulder, Co 80301, USA
7	Geonhwa Jee, Changsup Lee, and Jeong-han Kim
8	Korean Polar Research Institute
9	
10	Key Points
11	1. The stronger summer (northern) hemispheric power could be the cause of double hump in
12	the dayside meridional winds.
13	2. TIEGCM was able to reproduce the double-hump features seen by the HIWIND, and
14	single hump in the winter hemisphere observed at Jang Bogo.
15	3. TIEGCM overestimates the poleward wind on the dayside and equatorward wind on the
16	nightside in the summer hemisphere.
17	
18	Abstract
19	Using the HIWIND balloon and Antarctic Jang Bogo station high latitude conjugate observations
20	of the thermospheric winds we investigate the seasonal and hemispheric differences between the
21	northern and southern hemispheres in June 2018. We found that the summer (northern)
22	hemisphere dayside meridional winds have a double-hump feature, whereas in the winter (southern)
23	hemisphere the dayside meridional winds have a single hump feature. We attribute that to stronger

- summer, perhaps, northern hemisphere cusp heating. We also compared the observation with
- 25 NCAR TIEGCM (Thermosphere Ionosphere Electrodynamics General Circulation Model) model.
- The TIEGCM reproduced the double-hump feature because of added cusp heating. The summer
- 27 hemisphere has stronger anti-sunward winds. This is the first time we have very high latitude
- 28 conjugate thermospheric wind observations.

# Plane language abstract

29

35

36

37

38

39

40

41

42

43

44

45

46

- 30 Using balloon instrument in the northern hemisphere and ground based instrument in the southern
- 31 hemisphere, we study the conjugacy of the thermospheric winds of high latitudes. We found that
- 32 the more summer hemispheric heating alters the thermospheric winds and resulted in a double-
- hump feature on the dayside meridional winds. We also used model with cusp heating to simulate
- 34 the winds and were able to reproduce the double-hump feature.

#### Introduction

Inter-hemispheric conjugate observations are always very revealing about the intrinsic hemispheric differences and seasonal variations [e.g., Kosch et al., 2010; Wu et al., 2014. Wu et al., 2019c]. While for most ionospheric observation using radio wave method, seasonal variations at high latitude are not an issue for data coverage, it is an entirely different story for the optical remote sensing observations such as those of all sky camera and Fabry Perot interferometer (FPI) wind observations. Long polar summer daylight prevents any of these observations from the ground. That leaves large gap on the summer polar coverage. Only carefully selected time near equinox may provide some narrow windows for observations near the auroral zone as in the case analyzed by Kosch et al. [2010]. They used FPI instruments from northern Europe and Antarctica simultaneously observed conjugate thermospheric winds. Because of relative short nighttime on both ends of the conjugate points, the observation could not cover daily variation. Other conjugate

FPI observations are mostly performed in the mid latitudes [e.g., Wu et al., 2014; 2019c]. There are past studies using satellite observations of two hemispheres for inter-hemispheric comparison, most of them are based on statistical results and lack of instantaneous dynamic features [e.g., Luhr et al., 2007].

51

52

53

54

55

56

57

58

59

60

61

62

63

64

65

66

67

68

69

47

48

49

50

Conjugate comparison can show how the ionosphere thermosphere interacts during different seasons under nearly the same solar and geomagnetic conditions. The NASA supported HIWIND balloon FPI made a 5-day flight from Kiruna to northern Canada in June 2018, which finally provided much needed daytime summer thermospheric winds [e.g., Wu et al., 2012; 2019a, 2019b; Tan et al., 2022; Moe and Wu, 2014; Zhang et al., 2016]. The last two days of 2018 HIWIND was located at magnetic latitude about 75 degree, which was investigated by Wu et al. [2019b] and Tan et al. [2022]. In recent years, more FPIs have been deployed in the high latitudes [e.g., Wu et al., 2016]. In Antarctica, an NCAR built FPI [Wu et al., 2004] was deployed at Jang Bogo station (JBS, 74.6 S, 164.2 E, MLAT 77 S) in 2014. It has been taking thermospheric wind observations during nighttime for every austral winter season since then and have been used to study high latitude thermospheric winds [e.g., Wu et al. 2016]. During the HIWIND flight, the JBS FPI was operational. To examine how the HIWIND data can be related to the Antarctica data, we projected the HIWIND flight path onto the southern hemisphere according to the magnetic coordinates, which we will show in more detail later in the paper. It happens that the HIWIND projected path pass not far from JBS during the finally two days (180 and 181, June 29 and 30) of the flight. Hence, by pairing up the HIWIND and JBS observations we will have the first conjugate thermospheric wind observations in the high polar region. We will use the two data sets to examine the seasonal and hemispheric differences in the wind pattern in this paper. The paper is

organized as follows. We will give a brief description about HIWIND and JBS observations as well as models used in this paper. The results will be discussed and summarized.

72

73

74

75

76

77

78

79

80

81

82

83

84

85

86

87

88

89

90

91

92

70

71

#### **Observations and Models**

# HIWIND (High altitude Interferometer WIND experiment)

HIWIND is a NASA supported stratosphere balloon borne FPI for thermospheric wind observations, which had two successful flights in 2011 and 2018. It has a 10 cm aperture etalon [Wu et al., 2012]. The balloon was at about 40 km altitude during the flight, where the sunlight background was sufficiently low to allow daytime O 630 nm emission observation of the thermospheric winds. The balloon gondola orientation is controlled by a rotator, which locks the gondola solar panels to face the sun. The gondola maintained pointing with 1 +/- degree stability. The instrument took observations through four portholes in orthogonal directions. The integration The meridional and zonal winds are determined by decompose the time is 1 minute. measurements from the four orthogonal directions. The balloon orientation and speed are determined by the GPS compass. The balloon speed was removed in the data processing. During the 2018 flight, the HIWIND instrument obtained data from the high magnetic latitudes as shown in Figure 1. In search of the conjugate locations along the balloon flight path, the magnetic projection in the southern hemisphere (SH) is plotted in Figure 1b. We used the Apexpy to calculate the conjugate points along the HIWIND path [Emmert et al., 2010]. The balloon was launched on June 25, 2018 from Kiruna and the flight ended on June 30, 2018 just south of the Resolute. The balloon flight path maintained at roughly same geographic latitude as the balloon was carried westward by the prevailing stratospheric wind during the northern hemisphere (NH) summer season. Because of the Earth magnetic dipole offset the magnetic latitude of the balloon

gradually increase. Each of the days are marked with different colors. The SH conjugate projection passed the South Pole and near the Jang Bogo station. Because the Jang Bogo station had an operation FPI, we selected the day 180 and 181 (June 29 and 30) for conjugate study. The geomagnetic condition during the two days were very quiet (Kp < 1).

# JBO FPI

Jang Bogo station FPI has a 10 cm aperture etalon during the 2018 season, the instrument was operated in the 630 nm emission only mode. The instrument routinely samples winds at four cardinal directions with a 45-degree elevation angle and zenith. The integration time is 100 seconds. The wind errors are a few meters per second. The data have been used before for polar thermospheric wind study [e.g., Wu et al., 2016].

#### **TIEGCM Model**

We used two models to examine the conjugate thermospheric winds in comparison with the HIWIND and JBS observations. One is TIEGCM (Richmond et al., 1992). TIEGCM is a NCAR community model with fully incorporated equatorial electrodynamics. At high latitude the model is driven by the Weimer ion convection model [Weimer, 2005]. At the lower boundary of 97 km the TIEGCM is driven by the GSWM (Global Scale Wave Model) tidal climatology [Hagan and Forbes, 2002]. The simulation used in this study has a spatial resolution 2.5 deg and vertical resolution of 0.5 scale height. The simulated data are outputted at hourly interval.

#### **Observation and Simulation Results**

Figure 2 shows the observed thermospheric winds data from HIWIND and JBS on June 29-30, 2018 (days 180 and 181). Also shown are the simulation results at HIWIND locations and JBS from TIEGCM. The JBS data were shifted by 7 hours to match the JBS midnight with that of HIWIND at 19 UT. The sign of the meridional winds from JBS is reversed to make the interhemispheric comparison easier and the positive winds are poleward in both hemispheres. Local noon at HIWIND in the northern hemisphere is at 19 UT and midnight is about 7 UT.

In general, the winds from high latitudes have a strong diurnal variation in both zonal and meridional winds, which is the manifestation of the prevailing anti-sunward winds resulted from day/night pressure gradient and possible anti-sunward ion convection. In the case of the June 2018 data, the geomagnetic activity is very low [Tan et al., 2022], so the driving force of the anti-sunward winds are most likely from the pressure gradient.

Wu et al. [2019b] compared HIWIND data from Day 2018180 with TIEGCM simulations. Tan et al. [2022] have compared the data with TIEGCM simulations. The TIEGCM comparisons with the HIWIND in this paper are similar to that from Tan et al. [2022] and Wu et al. [2019b]. Wu et al. [2019b] focused on the nightside discrepancy between the TIEGCM simulation (overestimated anti-sunward) and the HIWIND observation. More soft electron precipitation was added to the TIEGCM and the discrepancy was reduced due to increase of the ionospheric density and ion drag in the polar cap. Tan et al. (2022) was mainly focused on the day-to-day variability of the HIWIND data in comparison with TIEGCM simulations.

The additional comparison with the JBS observation is new for this paper along with the TIEGCM simulation at JBS. And the focus of this paper is on the dayside meridional winds. The JBS data reveals some important insight about the seasonal variations of dayside thermospheric winds at high latitudes. On the dayside, the HIWIND meridional winds have a distinct double-hump feature (one at 12 UT day 180; and another at 3 UT day 181) whereas JBS showed a single hump feature at 19 UT and local noon day 180. This is one of the most important distinctions between the two hemispheres.

The TIEGCM JBS simulations showed a single hump feature for the wintertime southern hemisphere meridional winds. In the HIWIND comparison, the TIEGCM also showed double hump. Overall, the diurnal variation in the NH is larger than that in the SH from models and observations. As mentioned, the diurnal variation is a manifestation of the anti-sunward winds. The JBS FPI zonal winds in general were much less westward than those from HIWIND.

Figure 3 shows the vectors winds in local time from observations and simulations in the two hemispheres. In the northern hemisphere (Figure 3a), the dayside HIWIND winds showed smaller poleward winds relative to the TIEGCM. On the duskside, both HIWIND and TIEGCM show enhancement of poleward wind before turned equatorward. The duskside zonal wind from HIWIND and TIEGCM were westward showing mostly anti-sunward tendency. On the dawnside, the observations and simulations have better agreement, all show enhanced poleward wind then equatorward winds. The TIEGCM model overestimate poleward winds on the dayside and equatorward winds on the nightside compared to the HIWIND observations. HIWIND has noticeable westward wind on the dayside similar to the TIEGCM.

In the southern hemisphere (Figure 3b), the overall wind magnitudes are small than these in the northern hemisphere. TIEGCM overestimate the nightside winds and underestimate dayside winds. On the duskside and dawnside, the TIEGCM results have stronger equatorward winds than the JBS FPI observations.

#### **Discussions**

One of the key differences between the NH and SH is the location of the sunlight terminator. In the NH, the terminator is poleward of observation locations and equatorward in the SH. One should expect that the pressure gradient is larger on the dayside because of the heating gradient approaching the terminator. That is consistent with the simulations and observations of the two hemispheres, which show stronger diurnal variation in the NH than in the SH indicating stronger anti-sunward winds in the NH.

The difference in the dayside meridional wind is the double-hump (HIWIND) vs single hump (JBS) feature, which is due probably to the strong cusp heating in the summer hemisphere. At first we thought that cusp heating can produce density enhancement near the cusp blocking the poleward winds [Lühr et al., 2004; Moe and Wu, 2014]. The summer hemisphere tilts towards the sun can result higher particle influx and summer higher ionospheric conductivity can lead to stronger joule heating. CHAMP observations have shown that the summer cusp density enhancement is larger than that in the winter [Kervalishvili and Lühr 2013]. In addition, there are inter-hemispheric difference in cusp neutral density enhancement from the cusp heating [Lühr and Marker, 2013;

Rentz and Lühr, 2008], the SH density enhancement is shown to be smaller than that of NH. More cusp heating was added in the model to match HIWIND observations [Sheng et al. 2015].

Because the double-hump features extend passing dawn to 18 -22 LT, there are questions on whether cusp region is sufficiently large enough to influence the winds beyond dawn. We further examined the TIEGCM thermospheric temperature in both hemispheres during the local noon at HIWIND (June 29, 2018, Day 180, 19 UT) and Jang Bogo (June 30, 2018, Day 181, 01 UT). Figure 4 shows the thermospheric temperature in the two hemispheres. Because of the higher summer ionosphere conductivity, not only the cusp heating is enhanced, the overall hemispheric heating is higher compared to the winter hemisphere. The summer hemispheric power is twice of that in the winter [Luan et al., 2010]. As a result, the northern temperature has a plateau in the polar cap blocking the poleward thermospheric wind near local noon as shown in Figure 4. In the southern hemisphere, the temperature enhancement in the polar cap is weaker and not poleward of the JBS as in the case of HIWIND. Hence, there is not strong equatorward push from the temperature gradient at the local noon.

Figure 5 shows the potential map in the two hemispheres at the HIWIND local noon and JBS local noon. In the northern hemisphere, the HIWIND is on the dayside of the polar cap, the polar cap ion convection will pull the ion drift poleward in the meridional direction. In the southern hemisphere, because of the offset of the magnetic pole, the JBS is not at the dayside of the polar cap, rather it is in the dusk cell.

To further examine the ion drift and the temperature effect on the northern hemisphere meridional winds, we plotted the ion drift and negative temperature gradient in the meridional direction for the northern hemisphere (Figure 6). The convergence of the dawn and dusk convection cells near local noon formed a strong poleward ion drift plateau. The negative temperature gradient has a strong equatorward component centered at the local noon (highlighted by light-green color) will push the meridional in the opposite direction of the ion drift. Consequently, we see a valley in the meridional neutral wind forming a double-hump feature. Hence, we can see the double-hump is a results of strong heating in the polar cap and poleward ion drift. The large area of the polar cap leads to the humps to extend beyond local dawn and dusk.

Because of the unique capability of daytime wind measurement, HIWIND was able to offer this rare opportunity to examine the summer high latitudes and JBS happened to be in the right place to provide a good winter reference to see the seasonal contrast. The JBS zonal is less westward then HIWIND winds. That is because lower temperature in the winter polar cap can lead to smaller equatorward winds, which in turn lead to weaker westward wind from the Coriolis force.

Wu et al. [2016] made a comparison between ground based FPI observations from Resolute and JBS with the TIEGCM simulations and noted that the TIEGCM predicted much larger wintertime diurnal variations in meridional and zonal winds of the two hemispheres. In this paper, we see the same bias of the TIEGCM towards stronger anti-sunward winds.

# Summary

228 By combining this unique observational dataset from the two hemispheres, we are able to show 229 for the first time the significant hemispheric (seasonal) difference in the thermospheric winds: 230 1). The stronger summer (northern) polar cap heating could be the cause of a double-hump feature 231 in the summer dayside meridional winds in contrast with the single hump wintertime dayside 232 winds. 233 2). TIEGCM was able to reproduce the summer double-hump in the meridional winds and single 234 hump in the winter hemisphere consistent with observations. 235 3). TIEGCM overestimates the poleward wind on the dayside and equatorward wind on the 236 nightside in the summer hemisphere. 237 238 239 It is rare to see summer polar cap winds and HIWIND was able to clearly show the cusp heating effect and seasonal difference in the thermospheric winds. The observations can help further 240 241 improve understanding of polar cap thermosphere in different seasons and assess the performance 242 of the first principle model TIEGCM. TIEGCM performed pretty well. 243 244 **Open Research** 245 The HIWIND data can be found at https://spdf.gsfc.nasa.gov/pub/data/balloons/hiwind/. The JBS 246 FPI data, TIEGCM simulations used in the paper are provided by Wu et al. [2023]. 247 248 Acknowledgement 249 HIWIND project is supported by the NASA grant 80NAAC21K0014. Q. Wu is supported by 250 NASA grants 80NSSC20K0199, NNX17AG69G, NSF grants AGS-2120511 and AGS-2054356.

- 251 W. Wang is supported by 80NSSC20K0601, 80NSSC17K0013, 80NSSC20K0356,
- 252 80NSSC19K0080, 80NSSC17K0679, and 80NSSC20K0199. D. Lin is supported by
- 253 80NSSC17K0013, 80NSSC21K0008, 80NSSC20K0601, 80NSSC21K1677. L. Qian is supported
- by NASA grant 80NSSC20K0189. JBS is operated by Korean Polar Research Institute.

256

# References

- Emmert, J. T., A. D. Richmond, and D. P. Drob (2010), A computationally compact representation
- of Magnetic-Apex and Quasi-Dipole coordinates with smooth base vectors, J. Geophys. Res.,
- 259 115(A8), A08322, doi:10.1029/2010JA015326.
- Hagan, M. E., and J. M. Forbes (2002), Migrating and nonmigrating tides in the middle and upper
- atmosphere excited by latent heat releases, J. Geophys. Res., 107(D24), 4754,
- 262 doi:10.1029/2001JD001236.
- Kervalishvili, G. N., and H. Lühr (2013), The relationship of thermospheric density anomaly with
- electron temperature, small-scale FAC, and ion up-flow in the cusp region, as observed by
- 265 CHAMP and DMSP satellites, Ann. Geophys., 31(3), 541–554, doi:10.5194/angeo-31-541-2013.
- Kosch, M. J., et al. (2010), First observations of simultaneous interhemispheric conjugate high-
- 267 latitude thermospheric winds, J. Geophys. Res., 115, A09328, doi:10.1029/2009JA015178.
- Luan, X., W. Wang, A. Burns, S. Solomon, Y. Zhang, and L. J. Paxton (2010), Seasonal and
- 269 hemispheric variations of the total auroral precipitation energy flux from TIMED/GUVI, J.
- 270 Geophys. Res., 115, A11304, doi:10.1029/2009JA015063.

- Lühr, H., Rother, M., Köhler, W., Ritter, P., and Grunwaldt, L. (2004), Thermospheric up-welling
- in the cusp region: Evidence from CHAMP observations, Geophys. Res. Lett., 31, L06805,
- 273 doi:10.1029/2003GL019314.

- Lühr, H., Rentz, S., Ritter, P., Liu, H., and Häusler, K. (2007) Average thermospheric wind
- patterns over the polar regions, as observed by CHAMP, Ann. Geophys., 25, 1093–1101,
- 277 https://doi.org/10.5194/angeo-25-1093-2007.
- Lühr, H. and S. Marker (2013), High-Latitude Thermospheric Density and Wind Dependence on
- Solar and Magnetic Activity, 189-205 In F.-J. Lübken (ed.), Climate and Weather of the Sun-Earth
- 280 System (CAWSES), (189-205) Springer Atmospheric Sciences, DOI 10.1007/978-94-007-4348-
- 281 9 11.
- Merkin, V., & Lyon, J. (2010). Effects of the low-latitude ionospheric boundary condition on the
- 283 global magnetosphere. Journal of Geophysical Research: Space Physics, 115(A10). doi:
- 284 10.1029/2010JA015461.
- Moe, K., and Wu, Q. (2014), Impact of HIWIND balloon measurements on thermospheric density
- 286 models, J. Geophys. Res. Space Physics, 119, 2476–2483, doi:10.1002/2013JA019390.
- 287 Rentz, S., and H. Lühr (2008), Climatology of the cusp-related thermospheric mass density
- anomaly, as derived from CHAMP observations, Ann. Geophys., 26(9), 2807–2823,
- 289 doi:10.5194/angeo-26-2807-2008.

- 290 Richmond, A., Ridley, E., & Roble, R. (1992). A thermosphere/ionosphere general circulation
- 291 model with coupled electrodynamics. Geophysical Research Letters, 19(6), 601–604. doi:
- 292 10.1029/92GL00401.
- Sheng, C., Deng, Y., Wu, Q., Ridley, A. and Häggström, I. (2015), Thermospheric winds around
- the cusp region. J. Geophys. Res. Space Physics, 120: 1248–1255. doi: 10.1002/2014JA020028.
- Tan, Y., Dang, T., Lei, J., Zhang, B., Wang, W., Yang, Z., et al. (2022). Interplanetary control of
- 296 high-latitude thermospheric winds: Results from HIWIND and model simulations. Journal of
- 297 Geophysical Research: Space Physics, 127, e2022JA030394.
- 298 https://doi.org/10.1029/2022JA030394
- Toffoletto, F., Sazykin, S., Spiro, R., & Wolf, R. (2003). Inner magnetospheric modeling with the
- 300 rice convection model. Space Science Reviews, 107(1-2), 175– 196. doi:
- 301 10.1023/A:1025532008047.
- Weimer, D. R. (2005), Improved ionospheric electrodynamic models and application to calculating
- Joule heating rates, J. Geophys. Res., 110, A05306, doi:10.1029/2004JA010884
- Wu, Q., R. D. Gablehouse, S. C. Solomon, T. L. Killeen, C. She, Q. Wu, R. D. Gablehouse, S. C.
- 305 Solomon, and T. L. Killeen (2004), A new Fabry-Perot interferometer for upper atmosphere
- research, Proc. SPIE 5660, Instruments, Sci. Methods Geosp. Planet. Remote Sensing, (December
- 307 2004), doi:10.1117/12.573084.

- Wu, Q., Noto, J., Kerr, R., Kapali, S., Riccobono, J., Wang, W., and Talaat, E. R. (2014), First
- Palmer and Millstone Hill midlatitude conjugate observation of thermospheric winds, *J. Geophys.*
- 310 Res. Space Physics, 119, 3016–3028, doi:10.1002/2013JA019062.

- 312 Wu, Q., Wang, W., Roble, R. G., Häggström, I., and Strømme, A. (2012), First daytime
- 313 thermospheric wind observation from a balloon-borne Fabry-Perot interferometer over Kiruna
- 314 (68N), Geophys. Res. Lett., 39, L14104, doi:10.1029/2012GL052533.

315

- 316 Wu, Q., Jee, G., Lee, C., Kim, J.-H., Kim, Y. H., Ward, W., and Varney, R. H. (2016), First
- 317 simultaneous multistation observations of the polar cap thermospheric winds, J. Geophys. Res.
- 318 *Space Physics*, 122, 907–915, doi:10.1002/2016JA023560.

319

- Wu, Q. (2023), HIWIND Balloon and Antarctica Jang Bogo FPI High Latitude Conjugate
- 321 Thermospheric Wind Observations and Simulations, Dataset, GDEX,
- 322 <u>https://doi.org/10.5065/59tk-c632</u>.

323

- 324 Wu, Q., Knipp, D., Liu, J., Wang, W., Häggström, I., Jee, G., et al. (2019a). What do the new 2018
- 325 HIWIND thermospheric wind observations tell us about high-latitude ion-neutral coupling during
- 326 daytime? Journal of Geophysical Research: Space Physics, 124, 6173–6181.
- 327 https://doi.org/10.1029/2019JA026776

- Wu, Q., Knipp, D., Liu, J., Wang, W., Varney, R., Gillies, R., et al (2019b). HIWIND observation
- of summer season polar cap thermospheric winds. Journal of Geophysical Research: Space
- 331 *Physics*, 124, 9270–9277. <a href="https://doi.org/10.1029/2019JA027258">https://doi.org/10.1029/2019JA027258</a>

- Wu, Q., Sheng, C., Wang, W., Noto, J., Kerr, R., McCarthy, M., et al. (2019c). The midlatitude
- thermospheric dynamics from an interhemispheric perspective. *Journal of Geophysical Research*:
- 335 *Space Physics*, 124, 7971–7983. <a href="https://doi.org/10.1029/2019JA026967">https://doi.org/10.1029/2019JA026967</a>

336

- Zhang, B., Wang, W., Wu, Q., Knipp, D., Kilcommons, L., Brambles, O. J., Liu, J., Wiltberger,
- 338 M., Lyon, J. G., and Häggström, I. (2016), Effects of magnetospheric lobe cell convection on
- dayside upper thermospheric winds at high latitudes, Geophys. Res. Lett., 43, 8348–8355,
- 340 doi:10.1002/2016GL069834.
- Zhang, B., Sorathia, K. A., Lyon, J. G., Merkin, V. G., Garretson, J. S., & Wiltberger, M. (2019).
- 342 GAMERA: A three-dimensional finite-volume MHD solver for non-orthogonal curvilinear
- 343 geometries. The Astrophysical Journal Supplement Series, 244(1), 20. doi: 10.3847/1538-
- 344 4365/ab3a4c.

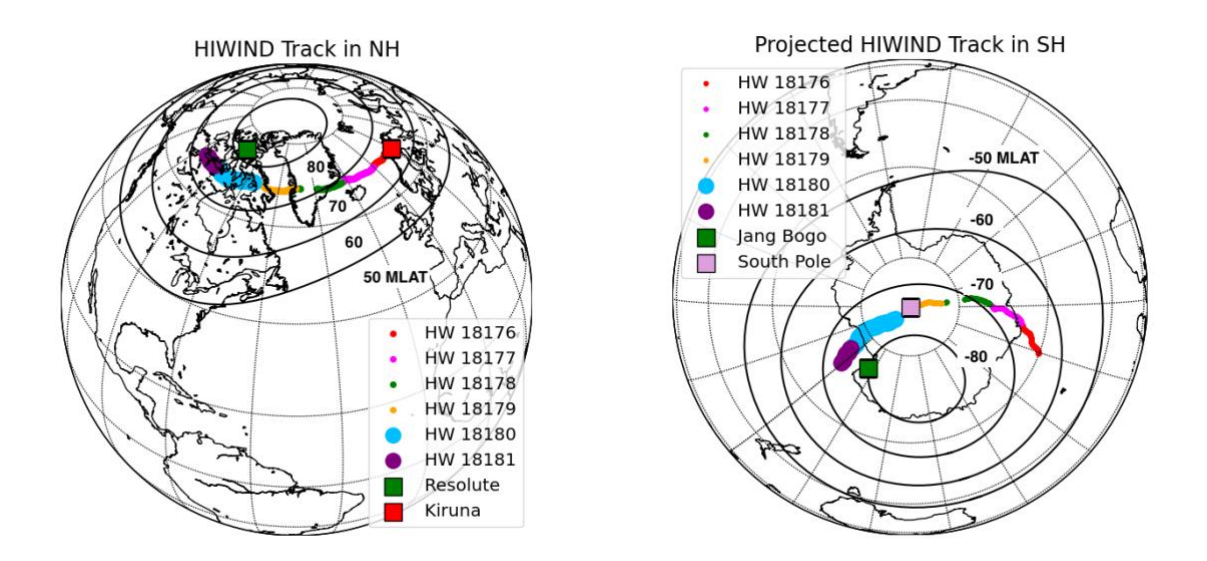


Figure 1. HIWIND 2018 flight path (left) and its projection in the southern hemisphere (right). The flight started on June 25, day 176 and ended on June 30, day 181. Each of the days are marked with different colors. The starting point Kiruna and a high latitude station Resolute are plotted for reference. The magnetic latitudes of 50, 60, 70, and 80 are also plotted. In the southern hemisphere, the flight path projection passed South Pole and went near the Jang Bogo station. Data from days 18180 and 18181 are used in this study, which are highlighted with thicker lines.

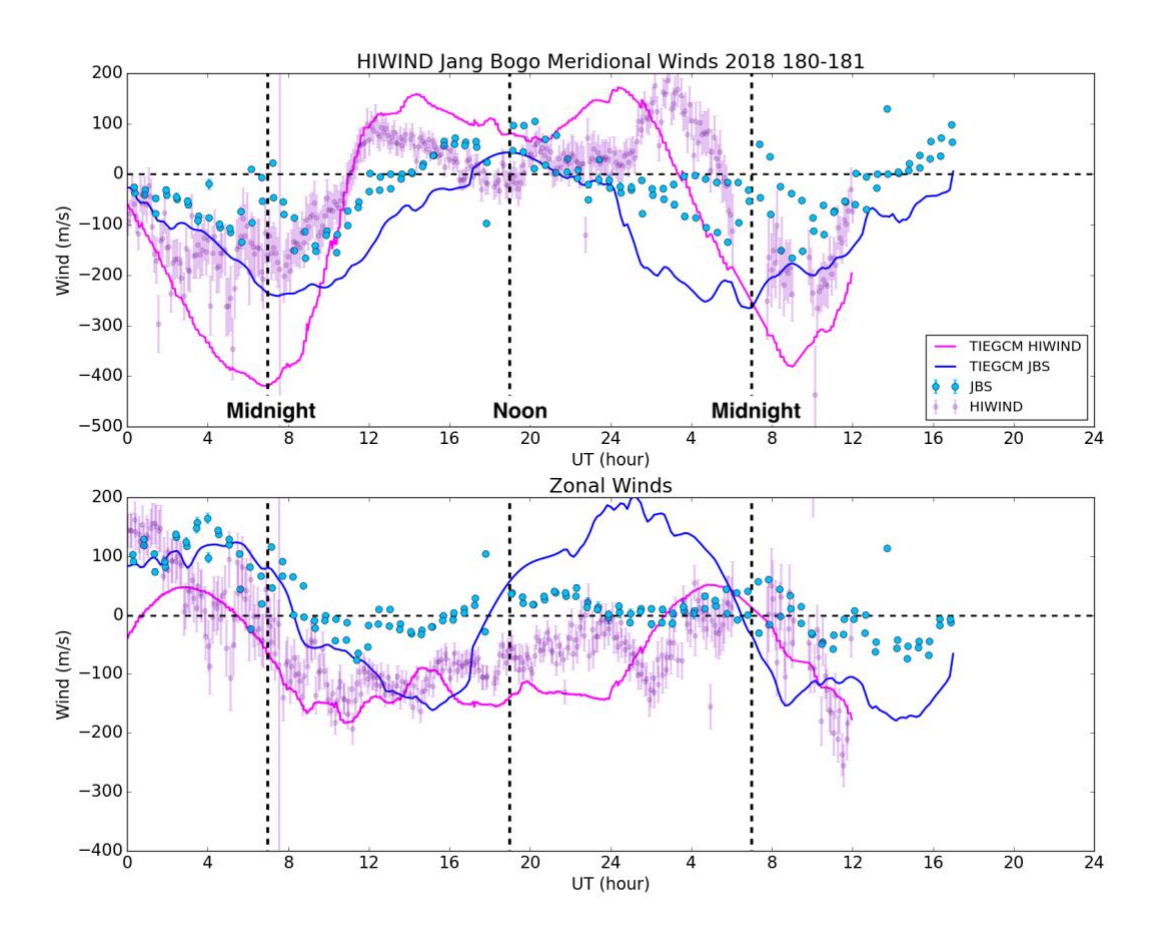


Figure 2. Thermospheric wind observations from HIWIND (northern summer) and JBS (southern winter) along with the TIEGCM simulations at the respective locations. The JBS data were shifted by 7 hours so that the local time of the JBS is approximately equal to that of HIWIND. The meridional winds from JBS were reversed so that the poleward meridional winds from JBS is positive for easy comparison with HIWIND data.

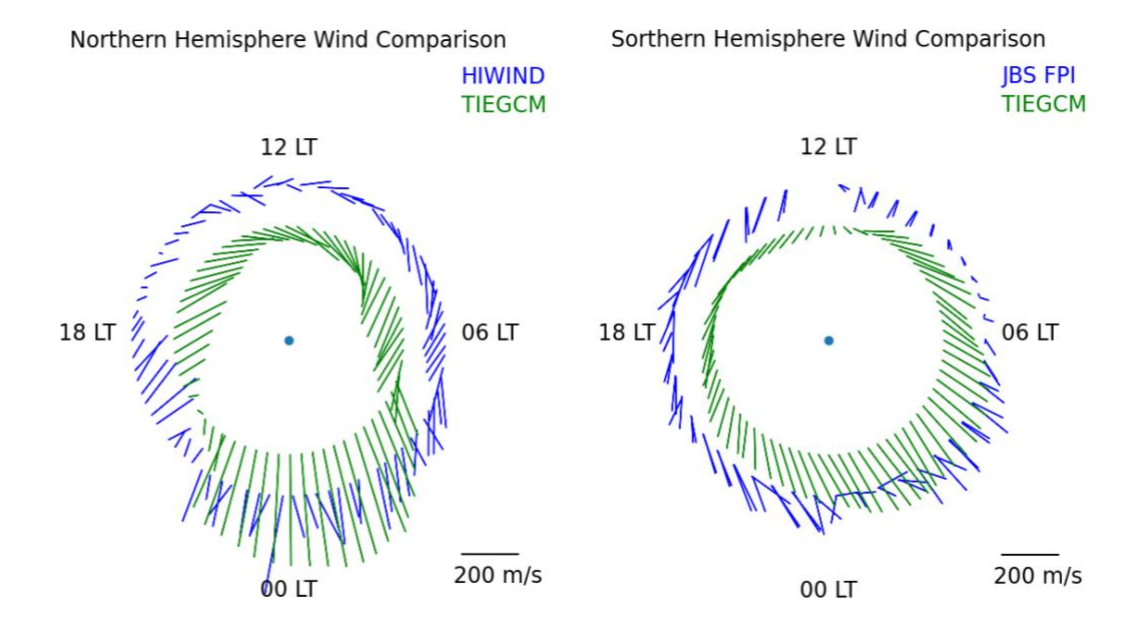


Figure 3 Vector wind plots for the northern and southern hemisphere observation and model comparison. The southern hemisphere plot is converted to the northern hemisphere convention for easy comparison.

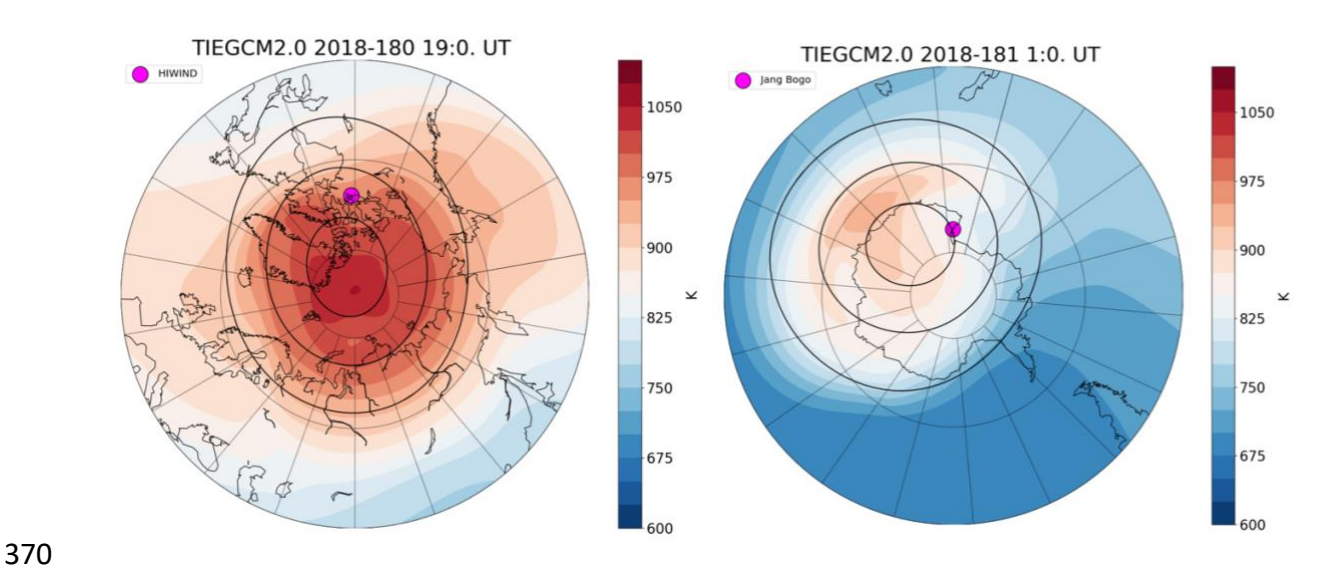


Figure 4. Thermospheric temperature in the northern (summer) and southern (winter) hemispheres. At local noon of HIWIND June 29, (day 180 19 UT), the HIWIND is just south of the polar cap, where the temperature is elevated. In the southern hemisphere at JBS local noon June 30 (day 181 1 UT), the polar cap is off to the side. Noon is at the top and midnight is at bottom. The dusk is on the left in the northern hemisphere and right in the southern hemisphere in each of the plots.

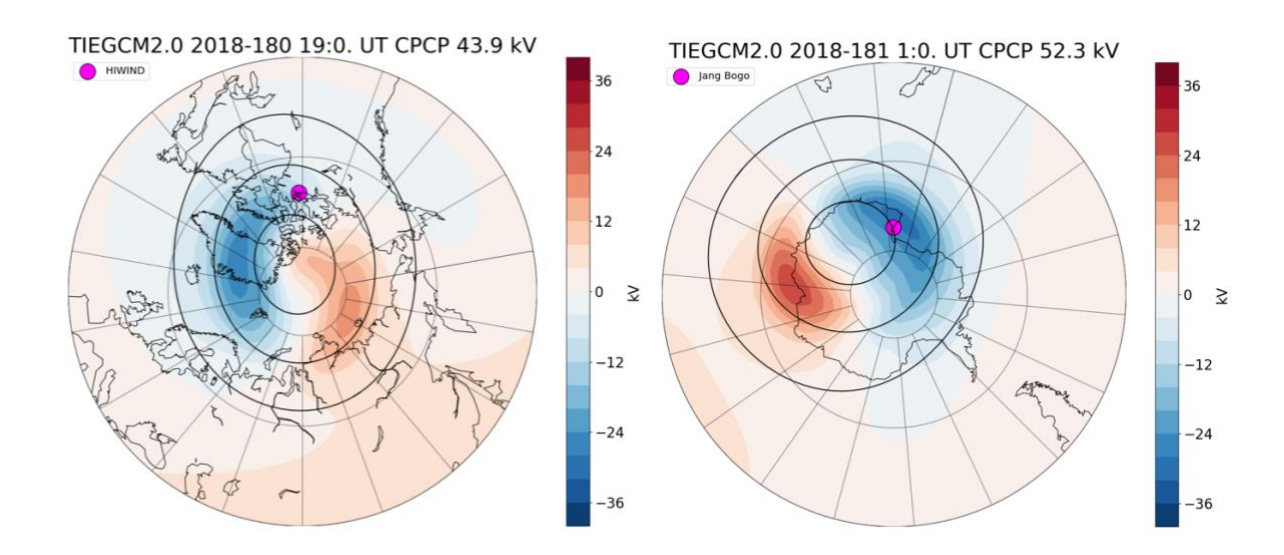


Figure 5. Potential maps of the two hemispheres at HIWIND local noon (left) and JBS local noon (right).

HIWIND Meridional Winds 2018 180-181

200

100

-200

-300

-400

4 8 12 16 20 24 4 8 12 16 20 22

UT (hour)

Figure 6. Meridional winds (magenta line TIEGCM; points HWIND), TIEGCM ion drift (green line), and TIEGCM negative temperature gradient (blue line) in the northern hemisphere. The highlighted area (light-green) indicates strong equatorward push from the negative temperature gradient on the polar cap edge.